

Experimental Characterization of the Mechanical Properties of 3D-Printed ABS and Polycarbonate Parts

Jason Cantrell¹, Sean Rohde¹, David Damiani², Rishi Gurnani³, Luke DiSandro¹, Josh Anton¹, Andie Young¹, Alex Jerez¹, Douglas Steinbach¹, Calvin Kroese¹, and Peter Ifju¹

¹Mechanical and Aerospace Engineering Department, 571 Gale Lemerand Dr., MAE-C 134, University of Florida, Gainesville, FL 32611

²Bartram Trail High School, Saint Johns, FL, 32259

³College of Engineering, University of California at Berkeley, Berkeley, CA 94720

Abstract

Purpose – This paper aims to present the methodology and results of the experimental characterization of three-dimensional (3D) printed ABS and polycarbonate (PC) parts utilizing digital image correlation (DIC).

Design/methodology/approach – Tensile and shear characterization of acrylonitrile butadiene styrene (ABS) and polycarbonate (PC) 3D-printed parts was performed to determine the extent of anisotropy present in 3D-printed materials. Specimens were printed with varying raster ([+45/-45], [+30/-60], [+15/-75], and [0/90]) and build orientations (flat, on-edge, and up-right) to determine the directional properties of the materials. Dogbone tensile and Isopescu shear specimens were printed and loaded in a universal testing machine utilizing 2D digital image correlation (DIC) to measure strain. The Poisson's ratio, Young's modulus, yield strength, ultimate strength, strain at failure, breaking strength, and strain energy density were gathered for each tensile orientation combination. Shear modulus, yield strength, and ultimate strength values were collected for each shear combination.

Findings – Results indicated that raster and build orientation had a negligible effect on the Young's modulus or Poisson's ratio in ABS tensile specimens. Shear modulus and shear yield strength varied by up to 33% in ABS specimens signifying that tensile properties are not indicative of shear properties. Raster orientation in the flat build samples reveal anisotropic behavior in PC specimens as the moduli and strengths varied by up to 20%. Similar variations were also observed in shear for PC. Changing the build orientation of PC specimens appeared to reveal a similar magnitude of variation in material properties.

Originality/value – This article tests tensile and shear specimens utilizing DIC which has not been employed previously with 3D-printed specimens. The extensive shear testing conducted in this paper has not been previously attempted and the results indicate the need for shear testing in order to fully understand the 3D-printed material behavior.

Keywords digital image correlation, 3D-printing, additive manufacturing, mechanical properties of materials, rapid prototyping, anisotropy, ABS, Polycarbonate

Paper type Research paper

Nomenclature

3D	= Three-dimensional
AM	= Additive manufacturing
ABS	= Acrylonitrile butadiene styrene
ASTM	= American Society for Testing and Materials
CAD	= Computer aided design
CI	= Confidence interval
COV	= Coefficient of variation
DIC	= Digital image correlation
FDM	= Fused deposition modeling
PC	= Polycarbonate
RP	= Rapid prototyping
SMP	= Shape memory polymer
STL	= Stereo lithography

1 Introduction

Fused deposition modeling (FDM) is an additive manufacturing (AM) technique which works by a heated nozzle laying down molten material in layers to produce a desired part. FDM is one of the most common techniques used for three-dimensional (3D) printers and has become one of the most popular rapid prototyping (RP) techniques in the last decade. FDM works by taking a part designed by a computer aided design (CAD) model exported as a stereo lithography (STL) file

and uploaded into a slicer program. The slicer program cross-sections the model into individual layers of a specified height and converts the desired height and other settings into G-Code to be read by the printer. The printer reads the G-Code, heats up a liquefier to the desired temperature to melt the polymer filament of choice, and begins extruding the material. The printing filaments used for this study were acrylonitrile butadiene styrene (ABS) and polycarbonate (PC). These filaments are fed through the heated liquefier by two drive wheels where the filament is then melted and extruded through a nozzle onto the build platform. The heating and extrusion of the filament to the specified diameter is all contained within the extrusion head which moves in the x-y plane depositing material on the build platform. A single line of material is called a road and the deposition of multiple roads side-by-side produces a single layer of a 3D-printed part. After each layer is finished the build platform moves down a specified z or layer height and the process repeats for the next cross-sectioned layer until the part is completed. Figure 1 illustrates this process and highlights some of key parts within the extrusion head as well as the deposition of the extruded filament.

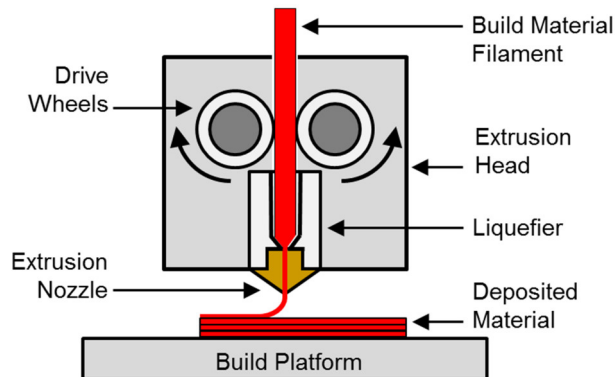


Figure 1. Schematic of the standard FDM process with callouts for select parts within the extrusion head

3D printing has increasingly progressed from a strictly prototyping technology to one used for production of final products intended for everyday use (Berman 2012; Chulilla Cano 2011; Espalin et al. 2014; Chua et al. 2003). 3D-printing has increasingly been used for advanced applications including the printing of adaptive structures utilizing shape memory polymer (SMPs) filaments and even printing cell structures in a granular gel medium (Ge et al. 2014; Ge et al. 2013; Raasch et al. 2015; Yang et al. 2015; Bhattacharjee et al. 2015). This explosion in popularity has come with a proportionate increase in the study of 3D-printed techniques as it is vital to comprehend the properties and characteristics of the parts which are created. Several previous studies utilized ASTM standard tensile test methods to determine the tensile properties as a function of the build and raster orientations the specimens were printed (Bellini & Güçeri 2003; Giannatsis et al. 2012; Hill & Haghgi 2014; Tymrak et al. 2014; Wittbrodt & Pearce 2015; Torrado Perez et al. 2014; Torrado et al. 2015; Es-Said et al. 2007; Ahn et al. 2003; Ahn et al. 2002; Montero et al. 2001). It has been widely publicized that in tension the road-to-road and layer-to-layer adhesion, shrinkage of the roads, and higher porosity in some orientations influences the material properties of the printed parts and causes anisotropy (Es-Said et al. 2007; Rodríguez et al. 2003; Torrado Perez et al. 2014). Several publications have worked to develop methods to reduce anisotropy including the creation of polymeric blends and other blended materials or post-processing the parts via radiation (Torrado Perez 2015; Shaffer et al. 2014; Torrado Perez et al. 2014; Torrado et al. 2015). Creating polymeric blends and other blended materials did tend to reduce anisotropy but at the cost of the overall material strength. Radiation tended to have mixed results as some temperature/radiation combinations resulted in weakening of the parts while others did reduce anisotropy. Other studies did offer a more in depth look at the anisotropic properties of 3D-printed materials and included the impact, flexural, or compression properties (Ziemian et al. 2012; Lee et al. 2007; Sood et al. 2010). However, most studies on anisotropy of 3D-printed materials generally give the Young's modulus, yield strength, and ultimate strength using extensometers and loads from a universal testing machine. These studies generally do not include other properties such as Poisson's ratio, strain energy density, or any shear data which are vital for complete understanding of the material behavior. Some publications did attempt to characterize shear properties of 3D-printed materials; however, these properties are limited to those determined from the tension tests using the elastic modulus and the Poisson's ratio (Ahn et al. 2003; Ahn et al. 2002; Montero et al. 2001). This approach assumes an isotropic relationship exists in the material on certain planes, which is somewhat of an over simplification. If the assumption is that the material is an-isotropic, which is why such tests are performed, this approach neglects to take into consideration the independence of the shear stress/strain behavior from the normal stress/strain behavior. Since the elastic moduli in all orientations don't vary significantly the assumption provides reasonably accurate shear moduli values. However, the shear strength as a function of orientation cannot be determined from tensile testing. In order to determine shear ultimate and yield strength a direct shear test method (specimen loaded in shear) should be utilized. Accurate shear strength measurements can only be made using a specimen that is loaded such that the test section is under both pure and uniform shear stress throughout the entire loading history. Pure shear means that normal stresses are minimized in the test section and shearing stresses

dominate. Uniform shear stress is required to insure that failure, both in yielding and ultimate, occurs through the entire test section as a whole and is not localized. The most pure/uniform loading condition for shear testing is a hollow cylindrical specimen loaded in torsion (Lee & Munro 1986). This however cannot be utilized in this study because the specimen geometry is based on a cylindrical coordinate system whereas the printed material is oriented in a Cartesian coordinate system.

There are direct shear test methods that are specifically designed to achieve pure and uniform shear loading. Examples include; Iosipescu test (Iosipescu 1967; Walrath & Adams 1983; Adams & Walrath 1987; Adams & Lewis 1995), Arcan test (Arcan 1973; Arcan et al. 1978), Single and double shear rail tests (ASTM International 2012; Whitney et al. 1971; Garcia et al. 1980). The Iosipescu specimen was designed for testing anisotropic materials, is the most widely accepted test method for composites and has been shown to provide accurate shear modulus, when instrumented properly, as well as shear strength. The specimen is also relatively compact and well suited for 3D-printed plastics. We propose to incorporate the use of the Iosipescu specimen for characterization of 3D-printed materials in order to measurement of shear modulus, shear yield stress and shear strength.

In order to accurately measure shear modulus the average shear stress at any load is determined by dividing the load by the original cross-sectional area of the sample test-section. Typically the shear strain is measured via electrical resistance strain gages; however for 3D-printed plastic materials gage reinforcement and self-heating complicate their use. Additionally, for this application with many dozens of specimens in our test program, application of electrical resistance strain gages would be prohibitively expensive and time consuming. We propose to utilize digital image correlation (DIC) a non-contact, full-field method instead (Sutton 2008; Sutton et al. 2009; Sutton et al. 1991). This methodology has been used on composites and plastics including PC and ABS; however, the studies on plastics were of injection molded specimens rather than 3D-printed parts (Fang et al. 2006; Fang et al. 2008; Daiyan et al. 2012; Qin et al. 2012). Using this experimental technique it is critical to measure the average shear strain in the test section rather than the shear strain at the center of the test section. This is because even though the specimen is designed to provide a uniform shear strain distribution in the test section, in reality the distribution is not perfectly uniform. The shear strain at the notches is zero, since it is a free surface with zero shear stress. The shear strain rises rapidly from the notches and forms a nearly uniform distribution. However the shear strain at the center of the test section does not equal the average value. Hence accurate shear stress/strain response can be determined by dividing the average shear stress by the average shear strain at any load, rather than by dividing the average shear stress by a local shear strain. This philosophy has been successfully utilized for composite material testing (Ifju 1994) using a specialized strain gage marketed by Vishay (Micro-Measurements Division 1995). In this study we will use DIC instead of strain gages similar to (Qin et al. 2012) to measure the average shear strains across the entire test section.

Since the load path in the Iosipescu specimen must be transferred through the test section and since the shear strain is measured in the test section and not globally (displacement of one side of the fixture with respect to the other) any yielding of the stress strain diagram is representative of the material behavior. Thus even if the specimen ultimately fails outside of the test section, the shear stress strain diagram is representative of the material behavior to that point. However the stress/strain response is cut short and the actual ultimate strength and percent elongation may be higher.

The tensile and shear tests methods in this study utilize the same universal testing machine and digital image correlation setup for efficiency. The normal strain in the dogbone tensile specimens are measured over an area near the center of both sides of the specimen, much like the shear tests, and thus compensates for bending about both vertical axis of the specimen. This methodology is adopted rather than cross-head displacement because the latter is susceptible to errors caused by grip slippage and compliance in the load cell and loading fixtures.

Both the tensile and dogbone specimens are printed in various orientations within the 3D-printer in order to assess the effect of build orientation and raster orientation on the anisotropy observed in the mechanical properties of ABS and PC test specimens. Both the ABS and PC specimens are evaluated for tensile and shear properties to give a complete picture of the mechanical behavior which will benefit researchers and undergraduates looking to incorporate 3D-printed parts into their respective projects. This paper will describe fabrication methods, experimental procedure, and results from the characterization of ABS and PC.

2 Fabrication methods, experimental set-ups, and procedures

2.1 Materials and specimen fabrication

The materials tested in this study were polycarbonate (PC) and acrylonitrile butadiene styrene (ABS) which were used to produce samples in a Stratasys® Fortus 360mc™ and an Ultimaker® 2 3D-printer respectively. The specimen geometries followed specifications outlined in ASTM D-638 for the Type IV tensile specimens and ASTM D-5379 for the shear specimens (ASTM International 2004; ASTM International 2011). These specimens and select dimensions for both specimen types are shown in Figure 2. Both specimen types were printed at a thickness of 4 mm (0.160 in). The shear and tensile specimens were first created in Solidworks®, exported in stereo lithography (STL) format, and then imported into each 3D-printer's respective slicer software to create the G-code used to print each specimen type.

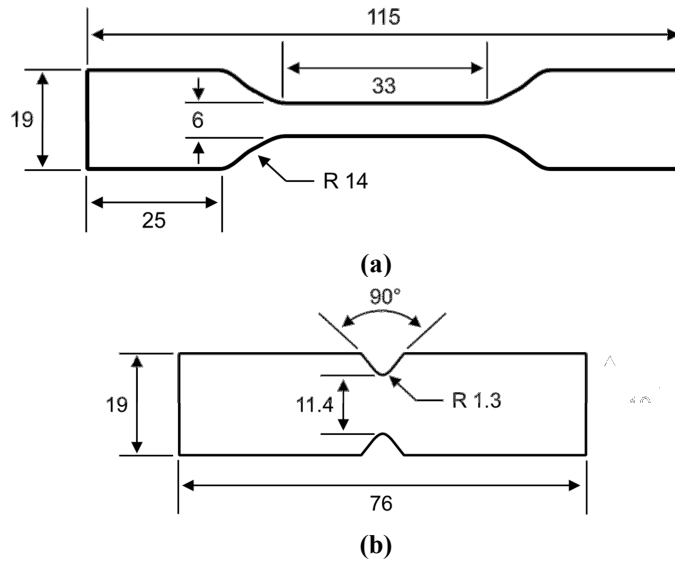


Figure 2. Schematic representation of the (a) ASTM D638 Type IV tensile specimen and (b) ASTM D5379 shear specimen geometries with relevant dimensions in mm

The specimens printed on the Fortus 360mcTM machine used an extrusion width (the width of each layer of deposited material, also known as the road width) of 0.508 mm (0.020 in) and a slice height (the height of an individual layer of deposited material) of 0.254 mm (0.010 in). The Ultimaker[®] 2 used a default slice height of 0.1 mm (0.004 in) and an extrusion width of 0.4 mm (0.016 in). The slice height, extrusion width, air gap (the space between the bead of material), printer environmental temperature (the temperature of the air around the part and the bed temperature), build temperature (the temperature of the liquefier), nozzle size (width of the hole through which the material is extruded), and color (white for ease of use with DIC which is discussed in detail later) were all held to constant values. The entire list of constant or default values used during this study are shown in Table I for each printer. In order to completely understand the design space used by the printers, both the layer extrusion path, otherwise known as raster orientation and the part build orientation were selected as the parameters to vary during testing. These parameters were determined to be the most important and have been investigated by several other authors (Bellini & Güçeri 2003; Montero et al. 2001; Tymrak et al. 2014; Smith & Dean 2013; Hill & Haghi 2014). The raster orientations selected for investigation were [+45/-45], [+30/-60], [+15/-75], and [0/90]. The majority of specimens were printed in the [+45/-45] or [0/90] raster orientations unless large difference in material properties were discovered for a specific orientation. These orientations were selected instead of unidirectional orientations as a majority of 3D-printers using an alternating raster pattern as the default printing scheme. Therefore, the data from this study will be directly relatable to the manufacturing of 3D-printed parts. In addition to the four raster orientations, three build orientations were also investigated. These orientations are based upon which plane the front face of the specimen resides and were named accordingly. The three orientations investigated were flat (XY plane), on-edge (XZ plane), and up-right (ZX plane) and for clarification purposes are illustrated in Figure 3 along with the raster orientation. An important item to note in Figure 3 is that the primary printing axis differs from the primary raster axis by an angle of 45°. When a sample is printed parallel to the X or Y build plane the printers default raster orientation is [+45/-45]. Therefore, when a sample is printed at a raster orientation of [0/90] the sample is positioned at an angle of 45° on the printer bed surface. Ten specimens were printed for each printer/raster orientation and the results for all ten tests averaged to find the properties in each orientation.

Table I. Constant 3D-printing process settings for the Fortus 360mcTM and Ultimaker[®] 2 printers

Parameter	Ultimaker [®] 2 ABS Value	Fortus 360mc TM PC Value
Air gap (mm)	0.0	0.0
Slice height (mm)	0.1	0.254
Extrusion width (mm)	0.4	0.508
Nozzle size (mm)	0.4	0.4
Filament color	White	White
Fill (%)	100	100
Liquefier temperature (°C)	235	345
Environmental temperature (°C)	105 (Bed)	145 (Ambient)

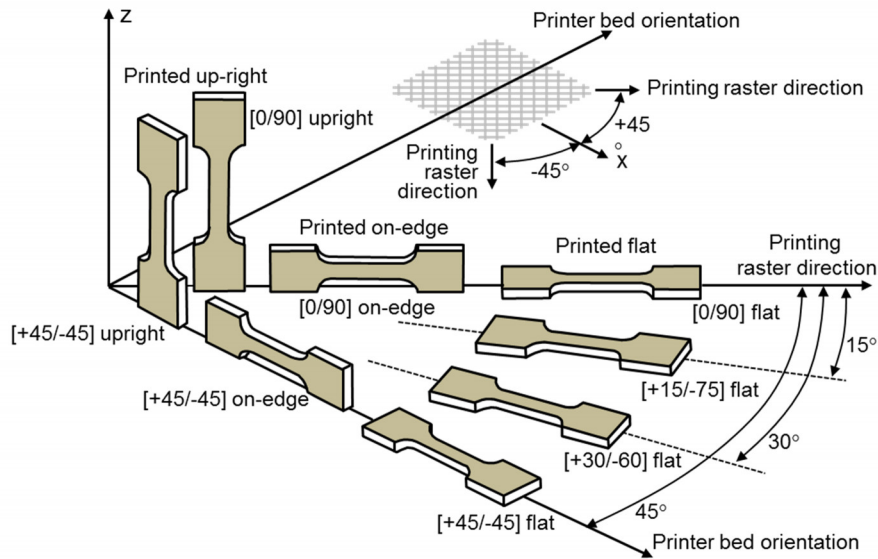


Figure 3. Graphic representation of the printer bed orientations (flat, on-edge, and up-right) and raster orientations ([+45/-45], [+30/-60], [+15/-75], and [0/90]) investigated

2.2 Testing machine and experimental set-up

A single test setup was developed for testing both tensile and shear properties of the material systems tested. The specimens were tested at a rate of 1.5 mm/min for both test methods at room temperature (~ 23 °C). Custom fixtures were manufactured to load the specimens in a Test Resources® 315 electromechanical universal testing machine equipped with a 22 kN load cell. The fixtures, shown in Figure 4a and Figure 4b, utilized multiple clevis joints to insure the load path through the sample was free of bending. Load values were recorded by Test Resources® Testbuilder™ software at a rate of 10 Hz. For tensile testing the average stress in the specimen, at any given load, was determined by dividing the load by the cross-sectional area. Collection of the necessary strain data was accomplished through the use of digital image correlation (DIC), a non-contact, full-field shape and deformation measurement technique. The strains were measured on both sides of the specimen using DIC over a rectangular region centered in the test section. This method compensates for a number of potential imperfections in loading and specimen geometry incurred during testing that cause inaccuracies. DIC was chosen for strain measurement rather than utilizing crosshead displacement because of potential grip slippage, loading mechanism compliance and load cell compliance, which is typical in such tests. Also, for testing polymers, electrical resistance strain gages mechanically reinforce the specimen as well as lead to strain gage self-heating issues. Additionally, extensometers typically only measure axial strain and in this study both axial and transverse strains are required to determine the Poisson's ratio. Although there are dedicated extensometers that measure both axial and transverse strain, such devices are bulky and the test section chosen for these studies is rather small. DIC strain measurement on both sides of the sample compensate for any bending during loading. Generally DIC can be performed either using a single camera or a pair in stereo. A single camera setup is susceptible to errors due to out-of-plane rigid body motion unless accounted for while the stereo setup can compensate for such motion. The DIC set-up used for this study consisted of two Point Grey® Research, 5-megapixel, grayscale cameras positioned on either side of the samples which simultaneously captured images of both sides of the samples. Using this single camera setup on both sides of the specimen allowed for compensation of rigid body motion by averaging the strain from the two sides. Specimen preparation only required a light speckle pattern of black paint over a light coat of white paint on the white plastic background, therefore had a negligible reinforcement effect. Images of the samples were captured via VIC-Snap™ 2009 at a rate of 1 Hz and later processed via VIC-2D™ to determine the strains. During processing in VIC-2D™ the standard subset size of 29 and step size of 5 were used which provided adequate strain and deformation data. After a sample was loaded into the testing machine and a preload applied, a pair of reference images (one image per camera) were taken of each side of the sample. These reference images were contrasted against images taken from the corresponding sides of the sample to determine the strains over the duration of the testing cycle. This methodology proved to be efficient and testing of a single specimen could be performed in a matter of minutes including mounting the specimen in the loading fixtures, taking initial undeformed DIC images, and loading the specimen through failure. The complete DIC and universal testing machine setup used for both tensile and shear testing is shown in Figure 4c.

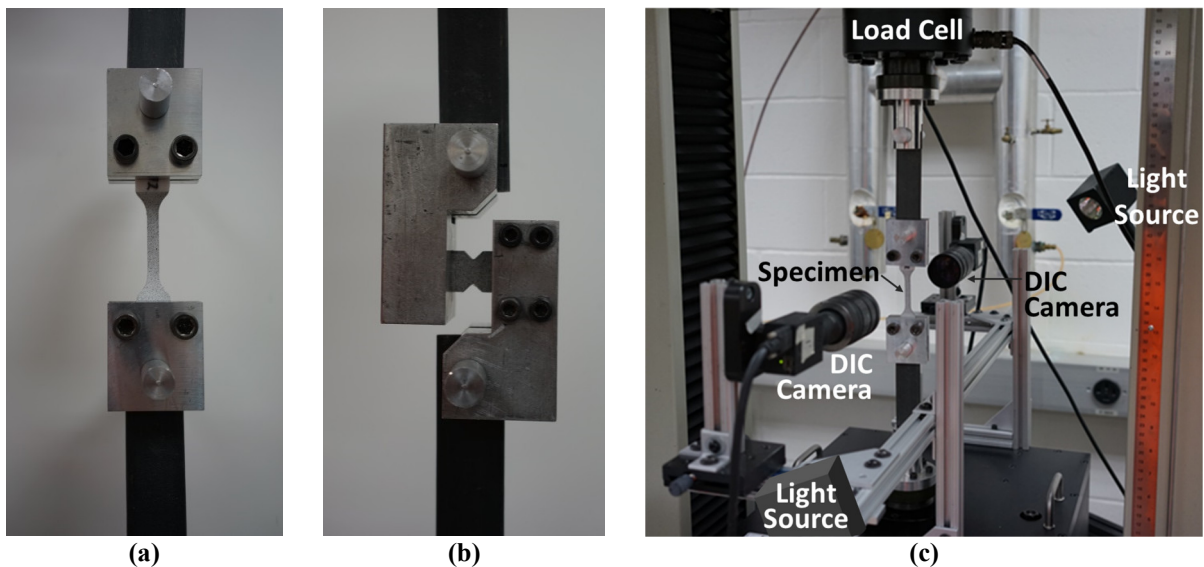


Figure 4. Photographs of the (a) tensile specimen fixture, (b) shear specimen fixture, and (c) the experimental set-up and DIC camera set-up

2.3 Experimental procedure

Each shear and tensile test followed the same general experiment procedure throughout this study. After applying the high contrast DIC speckle pattern to the sample, it is loaded into its respective shear or tensile fixture shown in Figure 4a and Figure 4b. Once the specimen is loaded into the fixture the fixture/specimen combination is secured into the Test Resources® testing machine with multiple clevis joints. A preload of ~ 10 N is then applied and reference images are taken of both sides of the sample via the VIC-Snap™ software. The testing machine is set to a displacement rate of 1.5 mm/min and the VIC-Snap™ DIC software set to a rate of 1 Hz. The DIC and testing machine systems are started simultaneously and the testing is conducted through specimen failure. After specimen failure the test is concluded and the process repeated. Once all ten tests in a data set are completed the stress and strain behavior is analyzed via a MATLAB script, relevant properties determined, and stress-strain curves created for each specimen or set of specimens. For the tension tests, the DIC images were analyzed to extract the average strain over a rectangular area of 3 mm wide by 7 mm long centered on the two faces of the specimen. This methodology provides a robust means to determine the average strain with good precision (repeatability). For the Iosipescu shear specimens the average shear strains on both sides of the specimen over a rectangular area of 3mm wide by 11 mm (almost spanning the entire distance between the notches) was analyzed, This method insured accurate and repeatable average shear strain results.

3 Experimental results

3.1 Tension

The tension specimens were tested in batches of ten printed for each printer/raster orientation and the results for all ten tests averaged to find the properties in each orientation. Previous literature was primarily concerned with Young's modulus, yield strength, and failure modes for tensile specimens (Montero et al. 2001; Hill & Haghi 2014; Giannatsis et al. 2012; Tymrak et al. 2014; Smith & Dean 2013; Wittbrodt & Pearce 2015; Torrado et al. 2015; Torrado Perez et al. 2014). However, to give better insight into the complete material behavior the breaking strength (strength at sample failure), strain at failure, and the strain energy density were all calculated for each sample set. Each of these material properties are highlighted in Figure 5 which illustrates where each property was calculated. The Young's modulus was calculated along the linear portion of the stress-strain curve, yield strength calculated using the 0.2% offset method, and ultimate strength at the maximum stress value acquired. Strain at failure was calculated from the last DIC image available before sample failure. Breaking strength corresponds to the stress at that failure strain. Strain energy density was calculated by integrating the specimen stress strain curve. All seven of these properties were evaluated for each orientation combination and the results presented below.

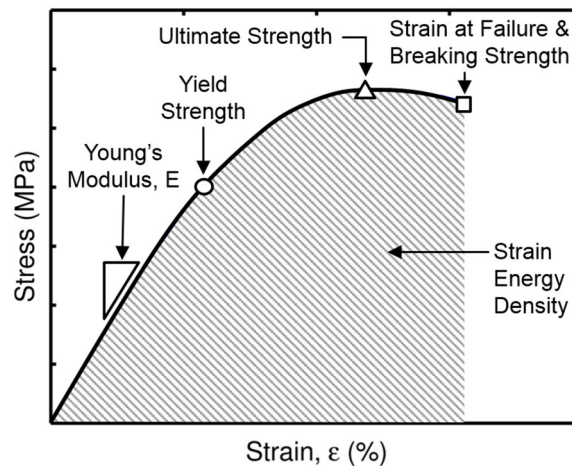


Figure 5. Illustration of the relevant tensile stress-strain properties evaluated during this study

The data from testing the ABS specimens showed some tensile properties appeared to behave isotropically while other properties exhibited anisotropic behavior with property differences of up to 91%. All of the ABS tensile properties evaluated and orientation combinations tested are presented in Table II. The Poisson's ratios and Young's moduli showed no statistically significant differences when comparing raster or print orientations as all values were within the 95% confidence interval (CI). When evaluating the yield strength of each combination the [0/90] flat specimens had the highest value and raster orientation appeared to affect yield strength in the flat build orientation as the [+45/-45] flat specimens were 5.3% weaker. Additionally, the [0/90] flat specimens had the highest ultimate strength; however, there were no statistically significant differences between the raster orientations. The up-right specimens had the lowest ultimate strengths and were on average 8% weaker than the flat specimens. The up-right printer orientations also had the lowest strains at failure, averaging 5.6% lower strain values than the flat orientation and 3.8% lower values than the on-edge orientations. Like the yield and ultimate strength values explained previously, the [0/90] flat specimens again had the highest breaking strength and was 3.6% higher than the [+45/-45] flat specimen. The only other statistically significant difference was between the [0/90] flat and on-edge specimens where there was a 0.1 MPa difference in the 95% confidence intervals and a 4.2% difference in the means. Finally, the property which exhibited the largest differences in values was the strain energy density. The flat orientations had the highest energy densities which were up to 91% higher than the up-right orientations and 54% higher than the on-edge orientations. Overall the [0/90] flat orientation had the highest tensile property performance while the [+45/-45] up-right orientation had the weakest properties. Anisotropy was found more often when varying printer orientation than when changing raster orientation and some ABS tensile properties exhibited isotropic behavior.

In addition to the results being detailed in Table II each tensile test was analyzed and plotted as a stress-strain curve to illustrate the data graphically. All ten tests from each orientation combination were plotted together to give an idea of the data spread and then averaged together to a representation of the typical stress-strain behavior for that combination. Two examples of the data scatter are shown in Figure 6a and Figure 6c. Figure 6a illustrates the relatively uniform behavior of the [+45/-45] flat ABS specimens through ultimate strength. The [+45/-45] flat specimens do have a large variation in strain at failure but have one of the lowest 95% CIs for breaking strength. Figure 6c shows the behavior of the [0/90] up-right specimens which have a confidence interval nearly twice as wide as the [+45/-45] specimens. Furthermore, the [+45/-45] flat specimens behave in a ductile manner while the [0/90] up-right specimens appear to behave in a more brittle manner as many specimens fail at the ultimate strength. This brittle behavior and higher CI is most likely due to the up-right printing orientation as failure strain is entirely dependent upon the adhesion between layers rather than the ABS roads themselves. The average specimen orientation behaviors shown in Figure 6b and Figure 6d respectively further illustrate these findings as the [+45/-45] specimen average has a clear ultimate strength peak followed by a long period of plastic deformation while the [0/90] specimen average has an elastic region quickly followed by failure of the specimens. Finally, all six orientation combinations are shown in Figure 6e which helps to visually present the entirety of the data displayed in Table II. The [0/90] flat orientation specimen clearly outperforms the other five orientation combinations with respect to strength, followed closely by the [+45/-45] flat, and then the on-edge orientations. The flat and on-edge orientations exhibit ductile material behavior while both up-right orientations behave in a brittle manner.

Table II. Tension properties and 95% CIs for the ABS specimen orientations tested

Property	Orientation					
	[+45/-45] flat	[0/90] flat	[+45/-45] on-edge	[0/90] on-edge	[+45/-45] up-right	[0/90] up-right
Poisson's Ratio	0.36 ± 0.03	0.37 ± 0.04	0.38 ± 0.03	0.36 ± 0.02	0.36 ± 0.03	0.36 ± 0.03
Young's Modulus (MPa)	1960 ± 60	2020 ± 60	2020 ± 110	1910 ± 60	2040 ± 90	2050 ± 110
Yield Strength (MPa)	30.3 ± 0.6	32.0 ± 0.8	30.0 ± 1.1	29.0 ± 0.6	29.3 ± 0.8	29.9 ± 1.6
Ultimate Strength (MPa)	32.8 ± 0.6	33.5 ± 0.5	31.9 ± 0.9	30.7 ± 0.7	30.0 ± 0.8	30.9 ± 1.3
Strain at Failure (%)	8.89 ± 2.34	7.14 ± 2.79	5.41 ± 1.13	5.82 ± 1.26	1.72 ± 0.16	1.84 ± 0.15
Breaking Strength (MPa)	29.6 ± 0.5	30.7 ± 0.5	30.1 ± 0.9	29.4 ± 0.7	29.9 ± 0.8	30.8 ± 1.3
Strain Energy Density (MJ/m³)	3.17 ± 1.04	2.14 ± 1.03	1.46 ± 0.37	1.66 ± 0.41	0.29 ± 0.04	0.32 ± 0.03

The data collected from the testing of the PC specimens, like the ABS specimens, showed that several tensile properties exhibited anisotropic behavior with property differences of up to 74%. The flat printer orientation presented such a large degree of anisotropy when varying raster orientation between [+45/-45] and [0/90] that two additional orientations ([+30/-60] and [+15/-75]) were printed to be evaluated resulting in a total of eight orientation combinations being tested for PC. All of the PC orientation combinations and their respective tensile properties are presented in Table III. The Poisson's ratio displays anisotropic behavior when evaluating raster orientation as the [+45/-45] flat orientation has a Poisson's ratio that is 26% higher than the [0/90] flat orientation. While not all Poisson's ratios in the flat printer orientation had statistically significant differences there was a pattern of increasing Poisson's ratio through the raster sweep from [0/90] to [+45/-45]. The same results were found when evaluating Young's modulus as the [+45/-45] flat orientation was 14% greater than the [0/90] flat orientation. The same increase in Young's modulus was found when sweeping through the raster angles in the flat orientation while the on-edge specimens appeared to be isotropic with respect to raster orientation. In the upright printer orientation anisotropic behavior was found as well as the [+45/-45] specimens had a Young's modulus that was 8% higher than the [0/90] specimens. Furthermore, there were significant differences between print orientations as the [+45/-45] on-edge had a 6% higher Young's modulus than the flat orientation and an 11.5% higher modulus than the up-right orientation. The [0/90] on-edge orientation had a 17% higher modulus than the other two print orientations whose moduli were approximately equal.

Anisotropic behavior was also present when evaluating the orientation combinations with respect to yield strength. Both the flat and on-edge orientations exhibited significant differences in raster orientation. The yield strength of the [+45/-45] raster specimen in the on-edge orientation was 8% higher than the [0/90] specimen. The [+45/-45] raster specimen in the flat orientation had a yield strength that was 14% higher than the [0/90] orientation and 23% higher than the [+30/-60] orientation. This was an unexpected result as the yield strength did not appear to correlate with the raster orientation and actually alternated through the raster sweep. Varying the printer orientation also resulted in statistically significant differences in yield strength as the on-edge print orientation was up to 21% greater than the up-right and up to 30% larger than the flat orientations. Ultimate strength and strain at failure yielded similar behaviors as the [+45/-45] raster orientations generally yielded higher ultimate strength and strain at failure values. Additionally, the same alternating pattern of material behavior was seen in the flat orientation with the [+45/-45] flat samples having 55% higher strain at failure values than [+30/-60] yet being only 30% higher than the [+15/-75] orientation. Breaking strengths were similar for the [+45/-45] and [+15/-75] flat orientations which were 23% higher than the breaking strengths of the [+30/-60] and [0/90] orientations. The on-edge specimens produced the highest breaking strengths while the upright specimens produced values similar to the weaker flat orientations. Finally, significant differences were seen in the strain energy density with respect to both the raster and print orientations. Again the on-edge orientations have much higher strain energy densities when compared to the up-right orientations. Overall the [+45/-45] on-edge orientation performed the best overall and had the highest or second highest tensile properties of the orientation combinations tested. The [+45/-45] flat and [0/90] on-edge orientations provided similar but slightly lower tensile properties. The on-edge specimens appeared to be isotropic in nature while large amounts of anisotropy were found when varying raster angle in the flat print orientation.

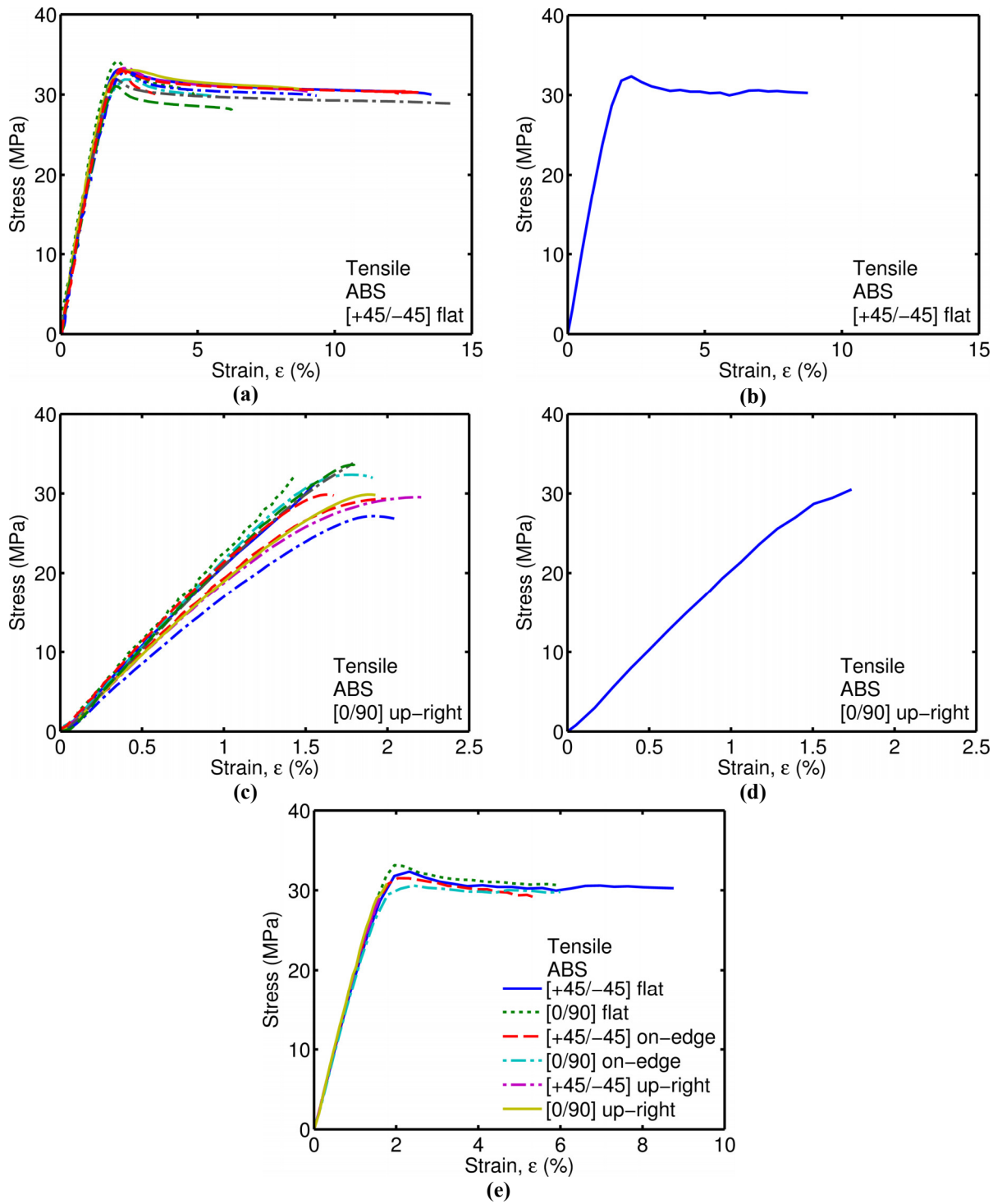


Figure 6. Stress-strain curves for (a) ten [+45/-45] flat ABS tension specimens illustrating the data scatter of the samples tested and (b) the average of the ten [+45/-45] flat ABS tension specimens. The stress-strain curves illustrating (c) the data scatter for ten [0/90] upright ABS tension specimens, (b) the average of the ten [0/90] upright ABS tension specimens, and (d) the six major ABS raster/print orientation combinations

Table III. Tension test results and 95% CIs for the PC specimen orientations tested

Property	Orientation			
	[+45/-45] flat	[+30/-60] flat	[+15/-75] flat	[0/90] flat
Poisson's Ratio	0.39 ± 0.03	0.36 ± 0.02	0.33 ± 0.02	0.29 ± 0.02
Young's Modulus (MPa)	1890 ± 60	1840 ± 20	1780 ± 30	1620 ± 60
Yield Strength (MPa)	39.7 ± 0.9	30.4 ± 1.3	38.8 ± 1.2	34.3 ± 1.5
Ultimate Strength (MPa)	56.6 ± 0.5	41.5 ± 2.3	54 ± 0.4	44.3 ± 0.4
Strain at Failure (%)	6.72 ± 0.94	3.01 ± 0.19	4.57 ± 0.07	3.78 ± 0.21
Breaking Strength (MPa)	54.0 ± 0.7	41.5 ± 2.3	53.7 ± 0.5	44.3 ± 0.4
Strain Energy Density (MJ/m ³)	2.91 ± 0.55	0.73 ± 0.09	1.49 ± 0.18	1.01 ± 0.08

Property	Orientation			
	[+45/-45] on-edge	[0/90] on-edge	[+45/-45] up-right	[0/90] up-right
Poisson's Ratio	0.37 ± 0.02	0.38 ± 0.03	0.35 ± 0.03	0.31 ± 0.02
Young's Modulus (MPa)	2000 ± 30	1950 ± 80	1770 ± 30	1630 ± 30
Yield Strength (MPa)	43.5 ± 1.1	40.0 ± 1.9	35.8 ± 0.6	34.5 ± 0.8
Ultimate Strength (MPa)	61.1 ± 0.5	57.9 ± 1.8	44.3 ± 1.1	42.4 ± 0.4
Strain at Failure (%)	6.03 ± 0.57	4.72 ± 0.44	3.07 ± 0.11	3.18 ± 0.05
Breaking Strength (MPa)	58.0 ± 1.4	57.8 ± 1.9	44.7 ± 1.2	42.2 ± 0.4
Strain Energy Density (MJ/m ³)	2.52 ± 0.19	1.75 ± 0.21	0.78 ± 0.06	0.76 ± 0.02

Generally the PC tests yielded confidence intervals and coefficients of variation (COVs) which were much smaller than the ABS specimens tested. The COV for the PC specimens averaged around 3.4% for the Young's modulus while the COV for ABS specimens was nearly double at 6.5%. This reduction in uncertainty was most likely due to the higher quality of the PC specimens printed by the Fortus 360mc™. This reduced scatter is clearly illustrated in Figure 7a as all ten [+45/-45] flat samples have almost identical stress-strain curves with the exception of the strain to failure behavior. Figure 7c shows the average behavior of the six primary orientation configurations which illustrates that the on-edge specimens outperform the other two printer orientations. The [+45/-45] flat orientation has properties similar to the on-edge specimens and then there is a marked decrease in moduli and strength properties when observing the remaining orientations. The on-side and [+45/-45] flat specimens exhibit a more ductile material behavior while the other three primary orientations behave in a brittle fashion. Finally, Figure 7d displays the raster sweep in the flat printer orientation which shows the discernible differences in material behavior with respect to raster orientation. The [+30/-60] and [0/90] orientations have much lower strength properties than the [+45/-45] and [+15/-75] orientations. The striking differences in material behavior could be due to a variety of factors like printer motor mechanics causing excessive air voids at the specimen boundaries or poor adhesion between PC layers.

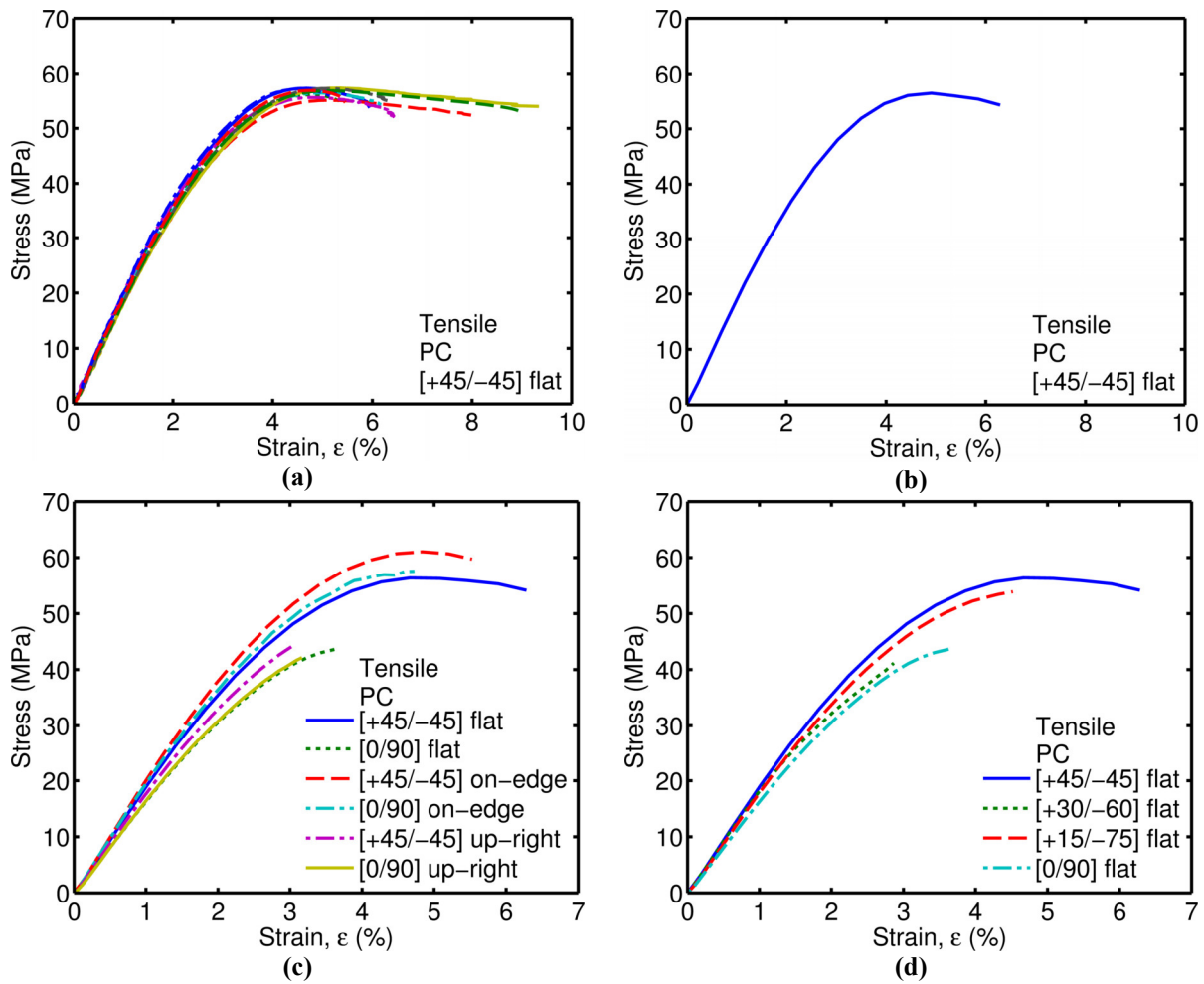


Figure 7. Stress-strain curves for (a) ten [+45/-45] flat PC tensile specimens and (b) the average of ten [+45/-45] flat PC tensile specimens. The average stress-strain curve behavior for (c) the six major PC raster/print orientation combinations and (d) a sweep of the flat PC raster orientations tested

While evaluating the PC and ABS specimens for the tensile material properties, the DIC images from each test were also evaluated to determine if patterns were present that could provide reasons for certain material characteristics. The PC specimens provided excellent DIC patterns and insight into material behavior; especially in the flat build orientation as individual PC roads in each layer could be seen when looking at the DIC results. Two sets of images depicting the longitudinal displacements and the strain fields for the [+45/-45] flat and [0/90] flat orientation combinations are shown in Figure 8. These images clearly show the loading conditions of the raster and the strain variations within each specimen. The [+45/-45] orientation specimen has a more uniform strain pattern with slight peaks in strain along the PC roads while the [0/90] flat orientation specimen has a bimodal strain pattern. The [0/90] specimen has an alternating pattern of 0% and 2.5% strain indicating that the individual roads are more likely to see higher strain values resulting in failure sooner than the more uniform [+45/-45] specimens where the entire structure is bearing the tensile load. This strain pattern also makes specimens more susceptible to failures due to printing imperfections as an imperfection could be printed along a road which would cause premature failure of the specimen due to the strain being concentrated in the individual roads. These observations support the results shown previously as the [0/90] flat specimens appear to perform worse than the [+45/-45] flat specimens in every tensile property category.

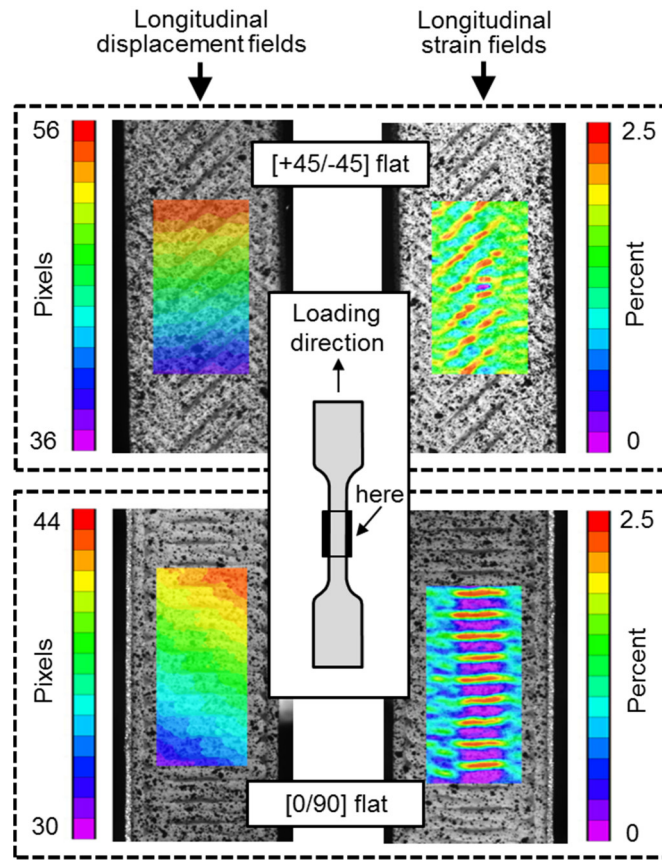


Figure 8. DIC results showing the longitudinal displacement and strain fields results for [+45/-45] and [0/90] flat PC tensile specimens

In addition to the stress-strain curve results, the fracture surfaces of the tensile specimens were evaluated for both the ABS and PC. The ABS specimens all behaved in a similar manner at fracture. These specimens all fractured cleanly in the plane perpendicular to the loading direction. The PC specimens fractured in a variety of ways and the most common failure modes for each orientation combination are shown in Figure 9. Most specimens appeared to fracture cleanly in the same perpendicular plane that the ABS samples did. However, there were some notable differences as both on-edge specimens had jagged perpendicular fracture surfaces. The [+45/-45] flat PC specimen was also notably different from most fracture surfaces as the PC roads tended to tear apart rather than break cleanly resulting in a saw tooth-like pattern. Overall the specimens that exhibited cleaner fracture surfaces had markedly lower strain at failure values when compared to the three previously mentioned specimen orientations. Additionally, these specimens had a lower Young's modulus, ultimate strength, and strain energy density. These results indicate that some insight into the overall material properties can be gained from simply observing the specimen failure modes.

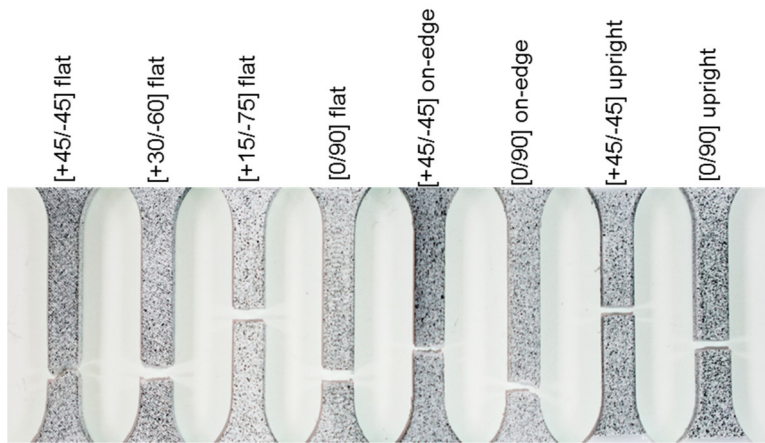


Figure 9. A photograph of gage sections of the eight tensile PC specimens and the most common failure modes for each raster/printer orientation combination

3.2 Shear

Like the results in the previous section, the shear specimen results were derived from ten tests for each printer/raster orientation and averaged to give a mean value as well as a 95% confidence interval for each parameter evaluated. The results of these tests are displayed in Table IV. During shear testing only the shear modulus, yield strength, and ultimate strength were calculated as some specimens did not fail before the destruction of the DIC speckle pattern, making strain to failure calculations for some samples impossible. The PC specimens were more apt to fail during testing while the ABS specimens were ductile and very few ABS specimens failed completely. Unlike the results seen in tensile testing, there were several cases of anisotropy seen during shear testing in the ABS specimens. Despite the Young's modulus appearing isotropic in nature during tensile testing, differences of up to 25% were found when comparing shear moduli. There was no significant effect on the shear modulus when varying raster orientation; however, when print orientation was varied the flat orientation was found to have a 25% higher modulus than the on-edge samples and 12% higher modulus than the up-right samples. The same results were seen when evaluating yield strength as raster orientation did not appear to have an effect on the sample strength. When evaluating printer orientation the flat orientations featured the highest values and the on-edge and up-right specimens being approximately equal in value. Finally, assessing the ultimate strengths revealed that the [0/90] on-edge specimens had 32% lower values than the [0/90] flat specimens. This dissimilarity appeared to be due to weak adhesion between the deposited layers of material as the [0/90] on-edge specimens appeared to delaminate along the notched area while most specimens had shear flow along the notched region. The ultimate strength of the up-right specimens was also lower than the flat specimens; however, no delamination occurred and the maximum difference was halved to 16%.

The PC specimens shear properties were much more varied and did see some anisotropy when comparing the orientation combinations. The [+45/-45] flat and [+45/-45] on-edge orientations had the highest shear moduli while the [0/90] flat orientation had the lowest modulus value. Raster orientation did have an effect on shear modulus as the [+45/-45] samples had the highest moduli values across all printer orientations. Printer orientation appeared to have less of an effect on shear modulus as only the [0/90] flat and [0/90] up-right specimens were significantly different from the other orientations. Yield strength and ultimate strength showed similar results when evaluating raster orientation as the [+45/-45] flat orientation yield strength was 36% higher and its ultimate strength was 20% higher than the [0/90] orientation. The exceptions were the on-edge samples, which were isotropic in nature. Overall the [+45/-45] flat orientation had the highest material properties while the on-edge printer orientation appeared to be the most isotropic. When sweeping through the raster angles in the flat orientation, all of the shear moduli were nearly identical with the exception of the [0/90] orientation. However, when evaluating the ultimate and yield strengths the same alternating pattern seen in the tensile results was also present in the shear samples. The highest values were seen in the [+45/-45] raster orientation, followed by the [+15/-75], [+30/-60], and [0/90] orientations respectively.

Table IV. Shear modulus, yield strength, and ultimate strength average values with 95% CIs for the ABS and PC specimen orientations tested

ABS			
Orientation	Shear Modulus (MPa)	Yield Strength (MPa)	Ultimate Strength (MPa)
[+45/-45] flat	740 ± 30	19.1 ± 0.5	28.8 ± 0.2
[0/90] flat	770 ± 40	21.5 ± 2.0	29.1 ± 0.3
[+45/-45] on-edge	610 ± 30	16.0 ± 1.1	23.9 ± 0.7
[0/90] on-edge	580 ± 20	14.5 ± 1.3	19.9 ± 1.8
[+45/-45] up-right	670 ± 30	15.5 ± 1.3	25.8 ± 0.3
[0/90] up-right	680 ± 40	15.4 ± 1.5	24.4 ± 0.5
Polycarbonate			
Orientation	Shear Modulus (MPa)	Yield Strength (MPa)	Ultimate Strength (MPa)
[+45/-45] flat	670 ± 10	22.8 ± 1.0	36.9 ± 0.3
[+30/-60] flat	640 ± 20	15.8 ± 0.6	30.4 ± 1.9
[+15/-75] flat	650 ± 20	18.2 ± 0.7	34.0 ± 0.8
[0/90] flat	540 ± 10	14.7 ± 0.8	29.5 ± 0.5
[+45/-45] on-edge	660 ± 10	19.9 ± 1.0	32.6 ± 0.7
[0/90] on-edge	650 ± 10	18.1 ± 0.9	30.0 ± 0.7
[+45/-45] up-right	680 ± 10	21.1 ± 0.6	34.0 ± 1.1
[0/90] up-right	630 ± 20	18.0 ± 0.6	30.0 ± 0.5

Images illustrating the scatter seen in the shear stress-strain curves and the average stress-strain behavior of ten [+45/-45] flat orientation ABS samples are shown in Figure 10a and Figure 10b respectively. The scatter and confidence intervals for the PC samples resulted in a Young's modulus COV of 3.5% while the ABS specimens produced an average COV of 7.7%, again nearly doubling that of the PC tests. Figure 10c shows the average behavior for the six primary orientation configurations for the ABS specimens. This figure helps to clearly illustrate the strength and superior properties of the flat orientation in shear. The up-right ABS specimens were the second best printer orientation and finally the on-edge specimens which appeared to perform poorly due to weak adhesion between the layers of material. Generally, the [+45/-45] specimens appeared to perform better in shear with the exception of the flat specimens were nearly identical. Figure 10d illustrates the average performance of the PC specimens in the six primary orientation configurations. The graph shows that [+45/-45] specimens are clearly superior specimens in shear as all three have ultimate values which are higher than the [0/90] specimens. There is less certainty when comparing printer orientation as in the flat configuration the [+45/-45] specimen has the best properties of the six specimens but the worst when oriented in the [0/90] orientation suggesting shear is more dependent upon raster orientation. Finally, Figure 10e presents the raster sweep in the flat printer orientation for the PC specimens. Again the results are mixed as the [+45/-45] configuration has the highest strength properties followed by the [+15/-75]. However, the moduli are similar for three of the four orientations despite the irregularity of the yield and ultimate strength properties.

Identical to the tensile testing procedure, DIC images were collected from each test to examine the strain fields during loading. The [+45/-45] flat and [0/90] flat orientation combinations showed some of the most noticeable patterns and images throughout the testing cycle. DIC results which display the longitudinal displacements and the strain fields at a point in the elastic portion of the stress-strain curve are shown in Figure 11. The images were taken at similar points in the stress-strain curve and clear patterns can be seen in both the [+45/-45] and [0/90] flat specimens. Both strain patterns show the road orientation within the specimen as the peak strains follow the roads. The difference in the specimens is, like in the tensile tests, the [0/90] specimen has an alternating peak and valley pattern while the strain appears to be more uniform in the [+45/-45] specimen. The [+45/-45] specimens strain is averaged over the entire specimen while the [0/90] specimen has concentrated loads at individual roads. These images support the outcomes shown previously as these concentrations appear to cause the [0/90] specimens to have a lower modulus and poorer strength values.

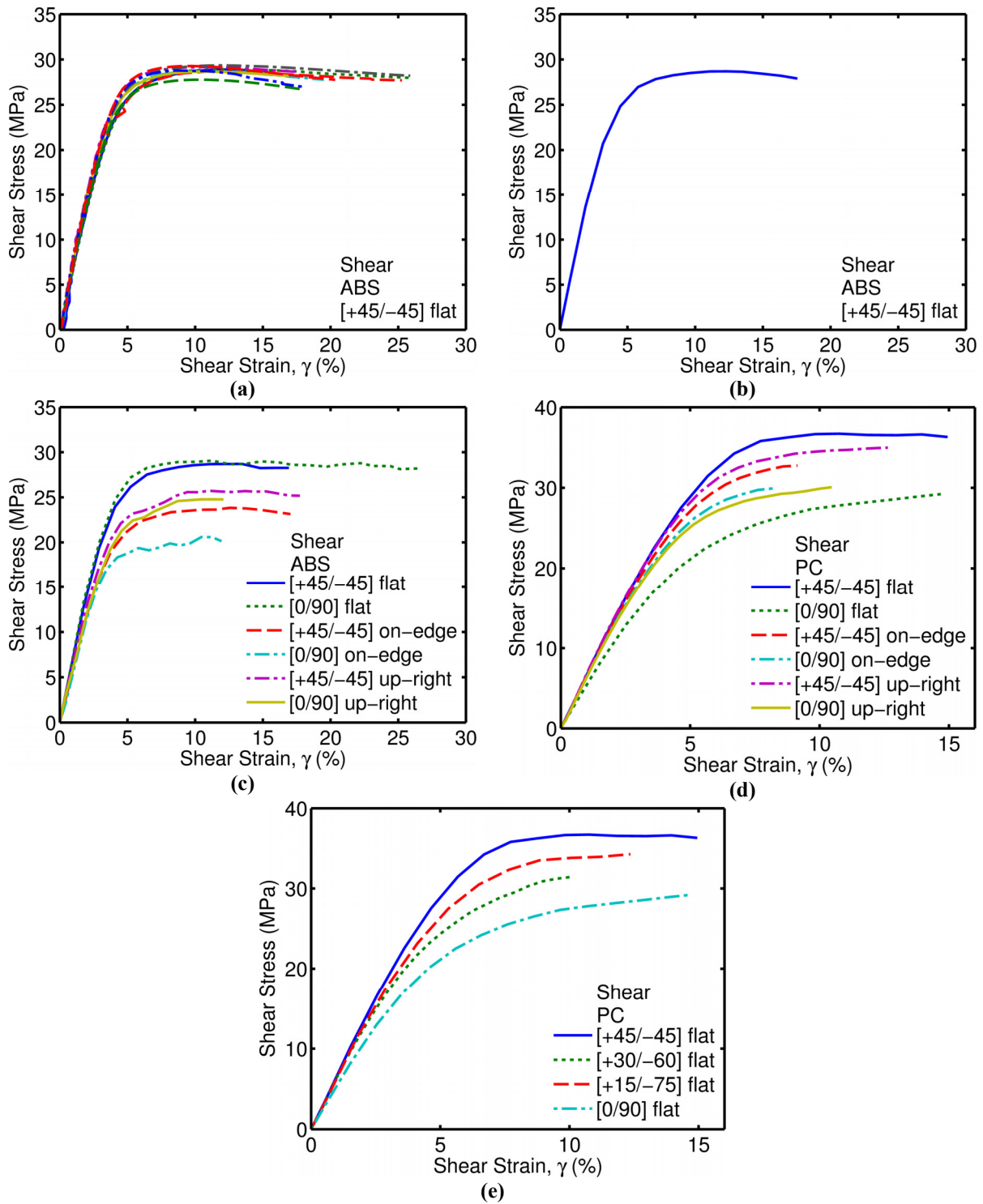


Figure 10. Stress-strain curves for (a) ten [+45/-45] flat ABS shear specimens illustrating the data scatter and (b) the average of ten [+45/-45] flat ABS shear specimens. (c) The average stress-strain curve behavior for the six ABS raster/print orientation combinations tested. The average stress-strain curve behavior for (d) the six major PC raster/print orientation combinations and (e) a sweep of the flat PC raster orientations tested

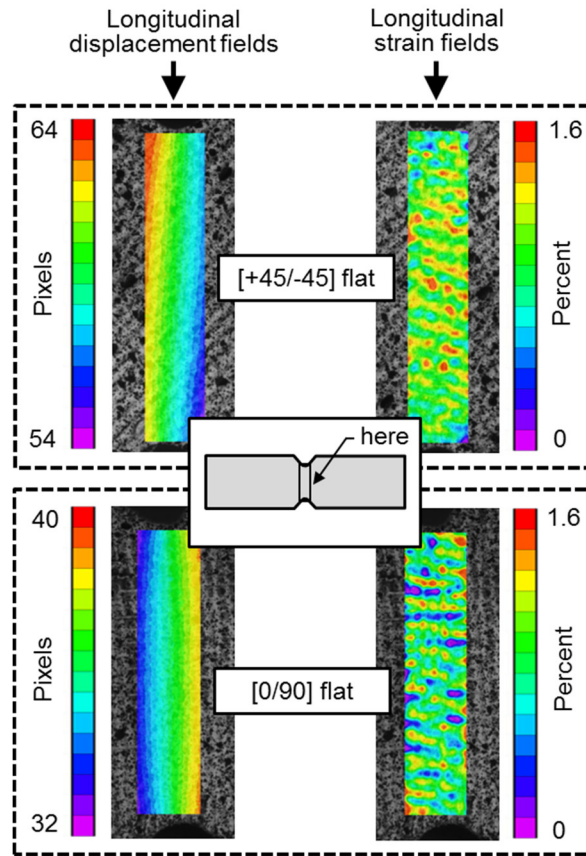


Figure 11. DIC results displaying the longitudinal displacement and strain fields for [+45/-45] and [0/90] flat PC shear specimens

Finally, the fracture surfaces of the shear specimens were also evaluated. Due to the ductile behavior of the ABS specimens very few specimens were brought to complete failure as destruction of the DIC speckle pattern occurred well before specimen failure. Therefore, the ABS specimens fracture surfaces were not evaluated. However, the PC specimens were much more brittle in nature, and nearly all specimens experienced complete failure during testing. The PC specimens fractured in two distinct ways which are pictured in Figure 12. Most specimens failed a short distance away from the notch on the tension side which is still considered a valid test as only the ultimate strength could be marginally affected by this type of failure. Far fewer specimens were observed to fail across the notch area and failure across the notch often indicated lower yield and ultimate shear strengths. The [+30/-60] and [0/90] flat samples saw the most specimens with failures in the notch area while the other orientations featured failures just outside the notch area.

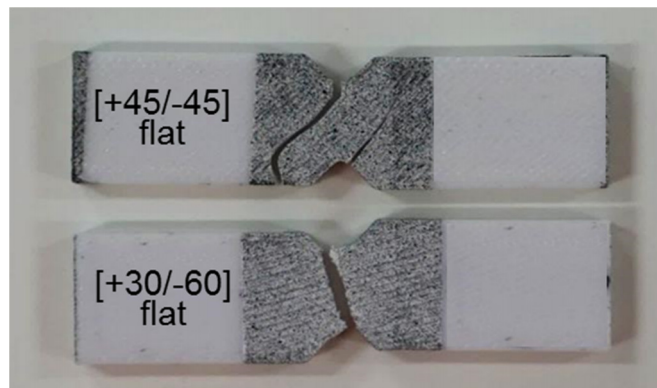


Figure 12. Typical failure modes seen during the testing of PC shear specimens

4 Conclusion

Polycarbonate (PC) and acrylonitrile butadiene styrene (ABS) specimens were created and evaluated according to ASTM standards D-638 (tensile) and D-5379 (shear) to determine if the specimens were anisotropic in nature. Four raster ([+45/-45], [+30/-60], [+15/-75], and [0/90]) and three build/printer orientations (flat, on-edge, and up-right) were selected to determine the directional properties of the materials. Images of the specimens during loading were captured via digital image correlation and processed to evaluate the properties of each raster and build orientation combination. The ABS specimens were isotropic in nature when comparing Young's modulus and Poisson's ratio; however, evaluating only these properties provides an incomplete and incorrect account of the behavior of ABS 3D-printed materials. Anisotropy was found when comparing the ultimate strength, strain at failure, and strain energy density of the ABS specimens. The largest degree of anisotropy found was when comparing the strain energy densities as the [+45/-45] flat orientation had a density that was 91% higher than the [+45/-45] up-right orientation. Raster orientation did not seem to affect the tensile and shear properties of the ABS specimens; however, printer orientation did appear to affect both the on-edge and up-right specimens. When evaluating the ABS shear specimens for anisotropy, differences of up to 25% were found when comparing shear modulus with similar dissimilarities in the shear strengths reported. Performance of the ABS specimens in tension was a poor indicator of performance in shear as properties varied significantly across the same orientation combinations.

The PC tensile specimens revealed large amounts of anisotropy when varying raster orientation in the flat and upright printer orientations while appearing nearly isotropic in the on-edge orientation. An additional sweep of the raster orientations in the flat build orientation revealed a linear increase in Poisson's ratio and Young's modulus when rotating from [0/90] to [+45/-45]. Strength and strain energy density showed mixed results as the [+30/-60] and [0/90] raster orientations performed significantly worse than the [+15/-75] and [+45/-45] orientations. The on-edge PC specimens had the highest overall tensile properties while the [+45/-45] flat orientation appeared to have the highest shear strengths. The shear modulus was nearly identical for all [+45/-45] raster orientations regardless of print orientation. Identical to the tensile results, the [0/90] flat orientation had the worst material properties with a shear modulus which was 18% lower than any [+45/-45] raster orientation. The PC specimens generally produced confidence intervals which were half the magnitude of the ABS specimens. This was likely due to the higher quality Fortus 360mc™ printer used to print the PC specimens. Overall specimens from both 3D-printers displayed large amounts of anisotropy when build and raster orientation were varied which cannot be ignored when producing or modeling 3D-printed parts.

References

- Adams, D. & Lewis, E., 1995. Current status of composite material shear test methods. *SAMPE*, 31(1), pp.32–41. Available at:
https://scholar.google.com/scholar?q=adams++lewis+current+status+of+composite+material+shear+test&btnG=&hl=en&as_sdt=0%2C10#0 [Accessed February 24, 2016].
- Adams, D.F. & Walrath, D.E., 1987. Further development of the losipescu shear test method. *Experimental Mechanics*, 27(2), pp.113–119.
- Ahn, S.H. et al., 2003. Anisotropic Tensile Failure Model of Rapid Prototyping Parts - Fused Deposition Modeling (FDM). *International Journal of Modern Physics B*, 17(08n09), pp.1510–1516.
- Ahn, S.-H. et al., 2002. Anisotropic material properties of fused deposition modeling ABS. *Rapid Prototyping Journal*, 8(4), pp.248–257.
- Arcan, M., 1973. A new method for the analysis of mechanical properties of composite materials. In *3rd International Congress on Experimental Mechanics*. Los Angeles, CA. Available at:
https://scholar.google.com/scholar?q=arcan+a+new+method+1973&btnG=&hl=en&as_sdt=0%2C10#0 [Accessed February 24, 2016].
- Arcan, M., Hashin, Z. & Voloshin, A., 1978. A method to produce uniform plane-stress states with applications to fiber-reinforced materials - A specially designed specimen yields material properties under pure shear or uniform plane-stress conditions. *Experimental Mechanics*, 18(4), pp.141–146.
- ASTM International, 2012. ASTM D7078/7078M-12 Standard Test Method for Shear Properties of Composite Materials by V-Notched Rail. , p.15.
- ASTM International, 2011. Standard Test Method for Shear Properties of Composite Materials by the V-Notched Beam Method. *Annual Book of ASTM Standards*, pp.1–13.
- ASTM International, 2004. Standard Test Method for Tensile Properties of Plastics. *Annual Book of ASTM Standards*, pp.1–15.
- Bellini, A. & Güçeri, S., 2003. Mechanical characterization of parts fabricated using fused deposition modeling. *Rapid Prototyping Journal*, 9(4), pp.252–264.
- Berman, B., 2012. 3-D printing: The new industrial revolution. *Business Horizons*, 55(2), pp.155–162. Available at:

<http://dx.doi.org/10.1016/j.bushor.2011.11.003>.

- Bhattacharjee, T. et al., 2015. Writing in the granular gel medium. *Science advances*, 1(8), p.e1500655. Available at: <http://www.pubmedcentral.nih.gov/articlerender.fcgi?artid=4643780&tool=pmcentrez&rendertype=abstract>.
- Chua, C.K., Leong, K.F. & Lim, C.S., 2003. *Rapid Prototyping: Principles and Applications, Volume 1*, World Scientific. Available at: <https://books.google.com/books?hl=en&lr=&id=hpNT01xw4EEC&pgis=1> [Accessed February 16, 2016].
- Chulilla Cano, J.L., 2011. The Cambrian Explosion of Popular 3D Printing. *International Journal of Interactive Multimedia and Artificial Intelligence*, 1(4), p.30.
- Daiyan, H. et al., 2012. Shear Testing of Polypropylene Materials Analysed by Digital Image Correlation and Numerical Simulations. *Experimental Mechanics*, 52(9), pp.1355–1369. Available at: <http://link.springer.com/10.1007/s11340-012-9591-7>.
- Espalin, D. et al., 2014. 3D Printing multifunctionality: Structures with electronics. *International Journal of Advanced Manufacturing Technology*, 72(5-8), pp.963–978.
- Es-Said, O.S. et al., 2007. Effect of Layer Orientation on Mechanical Properties of Rapid Prototyped Samples. *Materials and Manufacturing Processes*. Available at: <http://www.tandfonline.com/doi/abs/10.1080/10426910008912976> [Accessed February 18, 2016].
- Fang, Q.Z. et al., 2008. Effect of cyclic loading on tensile properties of PC and PC/ABS. *Polymer Degradation and Stability*, 93, pp.1422–1432.
- Fang, Q.Z., Wang, T.J. & Li, H.M., 2006. Large tensile deformation behavior of PC/ABS alloy. *Polymer*, 47, pp.5174–5181.
- Garcia, R., Weisshaar, T. a. & McWithey, R.R., 1980. An experimental and analytical investigation of the rail shear-test method as applied to composite materials. *Experimental Mechanics*, 20(8), pp.273–279. Available at: <http://link.springer.com/10.1007/BF02328411>.
- Ge, Q. et al., 2014. Active origami by 4D printing. *Smart Materials and Structures*, 23(9), pp.1–15. Available at: <http://stacks.iop.org/0964-1726/23/i=9/a=094007?key=crossref.b77e5da2653ac838509a57efc6aad683>.
- Ge, Q., Qi, H.J. & Dunn, M.L., 2013. Active materials by four-dimension printing. *Applied Physics Letters*, 103(13).
- Giannatsis, J. et al., 2012. Investigating the influence of build parameters on the mechanical properties of FDM parts. *Innovative Developments in Virtual and Physical Prototyping - Proceedings of the 5th International Conference on Advanced Research and Rapid Prototyping*, pp.525–529. Available at: <http://www.scopus.com/inward/record.url?eid=2-s2.0-84856713946&partnerID=tZOtx3y1>.
- Hill, N. & Haghi, M., 2014. Deposition direction-dependent failure criteria for fused deposition modeling polycarbonate. *Rapid Prototyping Journal*, 20(3), pp.221–227. Available at: <http://www.emeraldinsight.com/10.1108/RPJ-04-2013-0039>.
- Ifju, P.G., 1994. The Shear Gage: For Reliable Shear Modulus Measurements of Composite Materials. *Experimental Mechanics*, 34(4), pp.369–378.
- Iosipescu, N., 1967. New accurate procedure for single shear testing of metals. *J MATER*, 2(3), pp.537–566. Available at: https://scholar.google.com/scholar?q=iosipescu+1967&btnG=&hl=en&as_sdt=0%2C10#0 [Accessed February 24, 2016].
- Lee, C.S. et al., 2007. Measurement of anisotropic compressive strength of rapid prototyping parts. *Journal of Materials Processing Technology*, 187-188, pp.627–630. Available at: <http://linkinghub.elsevier.com/retrieve/pii/S0924013606011162>.
- Lee, S. & Munro, M., 1986. Evaluation of in-plane shear test methods for advanced composite materials by the decision analysis technique. *Composites*, 17(1), pp.13–22. Available at: <http://www.sciencedirect.com/science/article/pii/0010436186907299> [Accessed February 24, 2016].
- Micro-Measurments Division, M.G.I., 1995. Strain Gages for Shear Modulus Testing of Composite Materials.
- Montero, M., Roundy, S. & Odell, D., 2001. Material characterization of fused deposition modeling (FDM) ABS by designed experiments. *Proceedings of Rapid Prototyping & Manufacturing Conference*, pp.1–21. Available at: http://ode11.com/publications/sme_rp_2001.pdf.
- Qin, L. et al., 2012. Full-field analysis of shear test on 3D orthogonal woven C/C composites. *Composites Part A: Applied Science and Manufacturing*, 43(2), pp.310–316. Available at: <http://dx.doi.org/10.1016/j.compositesa.2011.11.006>.
- Raasch, J. et al., 2015. Characterization of Polyurethane Shape Memory Polymer Processed by Material Extrusion Additive Manufacturing. *Additive Manufacturing*. Available at: <http://linkinghub.elsevier.com/retrieve/pii/S2214860415000470>.
- Rodríguez, J.F., Thomas, J.P. & Renaud, J.E., 2003. Design of Fused-Deposition ABS Components for Stiffness and Strength. *Journal of Mechanical Design*, 125(3), p.545.
- Shaffer, S. et al., 2014. On reducing anisotropy in 3D printed polymers via ionizing radiation. *Polymer (United Kingdom)*, 55(23), pp.5969–5979. Available at: <http://dx.doi.org/10.1016/j.polymer.2014.07.054>.
- Smith, W.C. & Dean, R.W., 2013. Structural characteristics of fused deposition modeling polycarbonate material. *Polymer Testing*, 32(8), pp.1306–1312. Available at: <http://dx.doi.org/10.1016/j.polymertesting.2013.07.014>.
- Sood, A.K., Ohdar, R.K. & Mahapatra, S.S., 2010. Parametric appraisal of mechanical property of fused deposition

- modelling processed parts. *Materials & Design*, 31(1), pp.287–295. Available at: <http://linkinghub.elsevier.com/retrieve/pii/S0261306909002945>.
- Sutton, M.A. et al., 1991. Full-field Representation of Discretely Sampled Surface Deformation for Displacement and Strain Analysis. *Experimental Mechanics*, 31, pp.168–177.
- Sutton, M.A., 2008. *Springer Handbook of Experimental Solid Mechanics* W. N. Sharpe, ed., Department of Mechanical Engineering, Room 126, Latrobe Hall, The Johns Hopkins University, 3400 North Charles Street, Baltimore, MD 21218-2681, USA.
- Sutton, M.A., Orteu, J.J. & Schreier, H., 2009. *Image Correlation for Shape, Motion and Deformation Measurements: Basic Concepts, Theory and Applications*, Springer Science & Business Media. Available at: <https://books.google.com/books?hl=en&lr=&id=AlkqMxpQMLsC&pgis=1> [Accessed March 12, 2015].
- Torrado, A.R. et al., 2015. Characterizing the effect of additives to ABS on the mechanical property anisotropy of specimens fabricated by material extrusion 3D printing. *Additive Manufacturing*, 6, pp.16–29. Available at: <http://linkinghub.elsevier.com/retrieve/pii/S2214860415000111>.
- Torrado Perez, A.R., 2015. *Defeating Anisotropy in Material Extrusion 3D Printing Via Materials Development*. University of Texas at El Paso.
- Torrado Perez, A.R., Roberson, D.A. & Wicker, R.B., 2014. Fracture Surface Analysis of 3D-Printed Tensile Specimens of Novel ABS-Based Materials. *Journal of Failure Analysis and Prevention*, 14(3), pp.343–353. Available at: <http://link.springer.com/10.1007/s11668-014-9803-9>.
- Tymrak, B.M., Kreiger, M. & Pearce, J.M., 2014. Mechanical properties of components fabricated with open-source 3-D printers under realistic environmental conditions. *Materials and Design*, 58, pp.242–246. Available at: <http://dx.doi.org/10.1016/j.matdes.2014.02.038>.
- Walrath, D.E. & Adams, D.F., 1983. The Iosipescu shear test as applied to composite materials. *Experimental Mechanics*, 23, pp.105–110.
- Whitney, J.M., Stransbarger, D.L. & Howell, H.B., 1971. Analysis of the Rail Shear Test- Applications and Limitations. *Journal of Composite Materials*, 5, pp.24–34.
- Wittbrodt, B. & Pearce, J.M., 2015. The Effects of PLA Color on Material Properties of 3-D Printed Components. *Additive Manufacturing*. Available at: <http://linkinghub.elsevier.com/retrieve/pii/S2214860415000494>.
- Yang, Y. et al., 2015. 3D printing of shape memory polymer for functional part fabrication. *The International Journal of Advanced Manufacturing Technology*. Available at: <http://link.springer.com/10.1007/s00170-015-7843-2>.
- Ziemian, C., Sharma, M. & Ziemian, S., 2012. Anisotropic mechanical properties of ABS parts fabricated by fused deposition modelling. *Mechanical Engineering*, p.23. Available at: http://cdn.intechopen.com/pdfs/35261/InTech-Anisotropic_mechanical_properties_of_abs_parts_fabricated_by_fused_deposition_modelling.pdf.

Corresponding author

Jason Cantrell can be contacted at: jasoncantrell@gmail.com